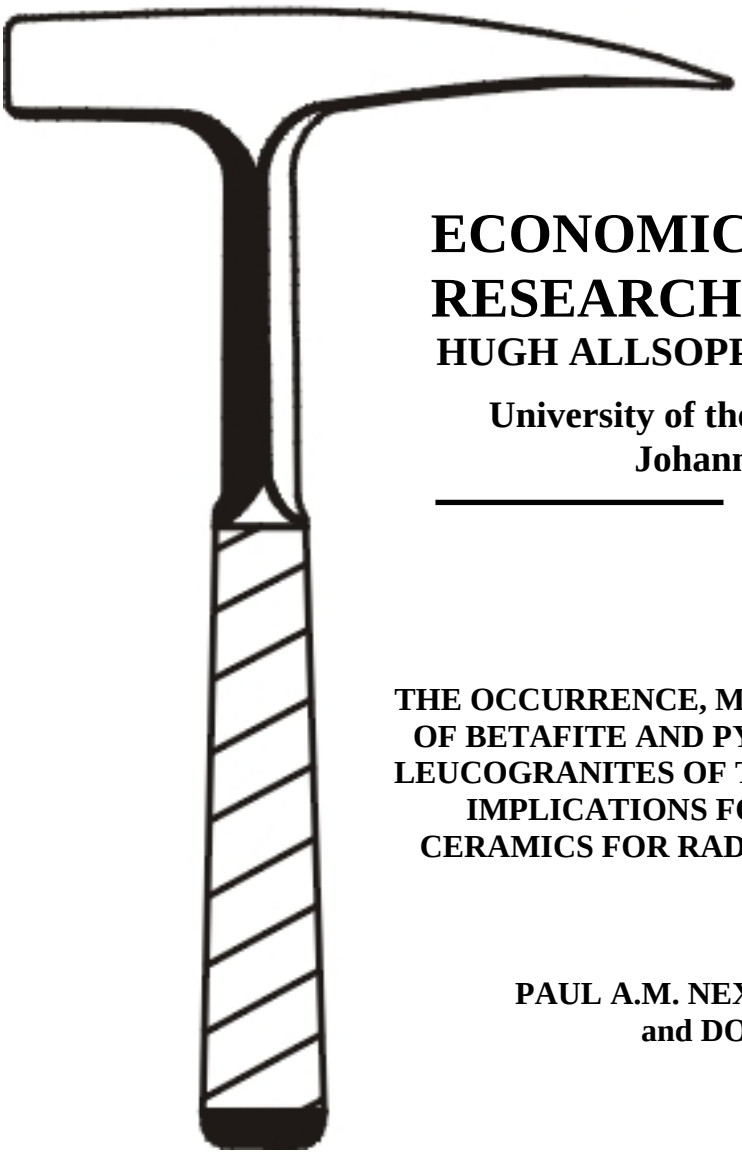

ECONOMIC GEOLOGY RESEARCH INSTITUTE

HUGH ALLSOPP LABORATORY

University of the Witwatersrand
Johannesburg

THE OCCURRENCE, MINERALOGY AND CHEMISTRY OF BETAFITE AND PYROCHLORE FROM SHEETED LEUCOGRANITES OF THE RÖSSING AREA, NAMIBIA: IMPLICATIONS FOR THE COMPOSITION OF CERAMICS FOR RADIOACTIVE WASTE DISPOSAL

PAUL A.M. NEX, JUDITH A. KINNAIRD and DONALD A. HERD

INFORMATION CIRCULAR No. 374

UNIVERSITY OF THE WITWATERSRAND
JOHANNESBURG

THE OCCURRENCE, MINERALOGY AND CHEMISTRY OF BETAFITE AND PYROCHLORE FROM SHEETED LEUCOGRANITES OF THE RÖSSING AREA, NAMIBIA: IMPLICATIONS FOR THE COMPOSITION OF CERAMICS FOR RADIOACTIVE WASTE DISPOSAL

by

PAUL A.M. NEX[1], JUDITH A. KINNAIRD[1] and DONALD A. HERD[2]

([1]Economic Geology Research Institute, School of Geosciences,
University of the Witwatersrand, Private Bag 3,
P.O. Wits 2050, Johannesburg, South Africa
[2]School of Geography and Geology, University of St. Andrews,
Fife, Scotland KY10 3HL)

ECONOMIC GEOLOGY RESEARCH INSTITUTE
INFORMATION CIRCULAR No. 374

December, 2003

THE OCCURRENCE, MINERALOGY AND CHEMISTRY OF BETAFITE AND PYROCHLORE FROM SHEETED LEUCOGRANITES OF THE RÖSSING AREA, NAMIBIA: IMPLICATIONS FOR THE COMPOSITION OF CERAMICS FOR RADIOACTIVE WASTE DISPOSAL

ABSTRACT

Three subgroups, betafite, pyrochlore, and microlite are classified according to atomic proportions of B atoms (Nb, Ti, Ta) such that betafite is classified as $2Ti \geq Nb+Ta$, and species are based on A atoms (Ca, Na, K, Sn, Ba, REE, Pb, Bi, U). In the Rössing area of Namibia, pyrochlore and betafite occur together as sparse accessories in sheeted leucogranites. There is a large variation in cationic species in both A- and B-sites and a considerable cation deficiency in the A-site for both betafite and pyrochlore. For pyrochlore, the B-site is dominated by Nb with some Ti and minor Zr. The A-site cation is predominantly Ca with lesser Y, Si, Fe, Th, U, Pb and Mn and A-site occupancy varies from 0.47 to 1.71. For betafite the B-site is dominated by Ti and Nb with minor W. The significant A-site cations are Ca and U with lesser Na, Y, Ce, Pb, Si, Fe, Mn and Th, with A-site occupancy varying from 0.88 to >2. Brown betafite has close to full site occupancy and <14.5 wt% REE's, whereas altered yellow betafite has > 1 atom per formula unit (pfu) vacancy and 1 - 3.5 wt%. This A-site vacancy in yellow betafite is linked to loss of Ca, Na and REE whereas the U has been retained. Artificial ceramics of betafite composition are, therefore, potential repositories for the containment of radioactive waste.

_____oOo _____

THE OCCURRENCE, MINERALOGY AND CHEMISTRY OF BETAFITE AND PYROCHLORE FROM SHEETED LEUCOGRANITES OF THE RÖSSING AREA, NAMIBIA: IMPLICATIONS FOR THE COMPOSITION OF CERAMICS FOR RADIOACTIVE WASTE DISPOSAL

CONTENTS

_____oOo _____

Published by the Economic Geology Research Institute
(Incorporating the Hugh Allsopp Laboratory)
School of Geosciences
University of the Witwatersrand
1 Jan Smuts Avenue
Johannesburg
South africa
http://www.wits.ac.za/geosciences/egri.htm
ISBN 1-86838-333-4

THE OCCURRENCE, MINERALOGY AND CHEMISTRY OF BETAFITE AND PYROCHLORE FROM SHEETED LEUCOGRANITES OF THE RÖSSING AREA, NAMIBIA: IMPLICATIONS FOR THE COMPOSITION OF CERAMICS FOR RADIOACTIVE WASTE DISPOSAL

INTRODUCTION

The Rössing Mine in Namibia produced 8.7 % of the world's uranium in 1999 (Crowson, 2001). Uranium-bearing ore has been commercially mined at Rössing since 1978. The open cast pit measures 2 km by 1 km in size and is over 300 m deep (Fig. 1). The primary ore mineral is principally uraninite although a substantial amount of uranium is also recovered from secondary uranium minerals. In addition, uranium is found in betafite and other pyrochlore-group minerals in the Rössing area. Although a relatively rare mineral, betafite, a Ti-rich pyrochlore, is a widespread accessory mineral in some of the abundant leucogranite sheets of the Rössing Uranium Mine (Fig. 2). Because betafite is not soluble in the acid-leach processing, the uranium content of betafite is lost to the tailings. This paper presents results of part of a project undertaken to assess the abundance and distribution of betafite in the environs of the Rössing Mine.

Figure 1. *Photograph of the Rössing Mine looking eastwards. Khan Formation pelitic metasediments of the footwall form the north face of the pit.*

However, the fact that betafite retains actinides within its structure, even after alteration, is of fundamental significance in the nuclear industry. Studies of natural betafite may have direct application to the titanite ceramic designed for disposal of partially reprocessed nuclear fuel elements (Ball *et al.*, 1989). Thus the study of betafite is of much more than local interest.

PYROCHLORE GROUP CLASSIFICATION

Betafite was first described from granitic pegmatites at Betafo, Madagascar (Lacroix, 1912). It is the Ti-rich member of the pyrochlore group, which comprises pyrochlore (ss), betafite and microlite (Hogarth, 1977, 1989).

Figure 2. *Uranium-bearing sheeted leucogranites intruding Khan Formation metasediments in the vicinity of the Rössing Mine.*

According to Hogarth (1989) pyrochlore has the group cell-formula:

$$A_{16-x}B_{16}O_{48}(O,OH,F)_{8-y}\cdot {}_zH_2O$$

where *x* and *y* are vacant sites in the unit cell, *z* indicates variable degrees of hydration and *x*, *y*, and *z* are non-rational. *A* atoms which occupy the 'cubic site' may include As, Ba, Bi, Ca, Cs, K, Mg, Mn, Na, Pb, REE's, Sb, Sn, Sr, Th U, and Y. The *B* atoms fill the 'octahedral site' in the structure and include Nb, Ti and Ta plus Zr and W. The pyrochlore group has the space group Fd3m and an $E8_1$ structure as defined by Gaertner (1930) and Brandenberger (1931). The three subgroups of the pyrochlore group (pyrochlore, betafite and microlite) are classified according to atomic proportions of *B* atoms while subgroup species are classified according to *A*-site atoms (Table 1). Betafite was defined by the pyrochlore subcommittee of the IMA Commission on Mineral Names as containing $2Ti \geq Nb+Ta$ (Hogarth, 1977, 1989).

Table 1: Subgroups and species of the pyrochlore group (from Hogarth, 1977, 1989)

Subgroups defined by *B* atoms i.e. Nb, Ta, Ti			PYROCHLORE sub-group Nb+Ta >2Ti Nb >Ti	MICROLITE sub-group Nb+Ta >2Ti Ta ≥Nb	BETAFITE sub-group 2Ti ≥Nb+Ta
Species defined by *A*-atoms K, Sn, Ba REE, Pb Bi, U	Na+Ca but no other *A*-atoms > 20% total *A*-atoms		pyrochlore	microlite	calciobetafite
	One or more *A*-atoms other than	K	kalipyrochlore		
	Na or Ca, > 20% total *A*-atoms	Cs		cestibtantite	
		Sn		stannomicrolite	
		Ba	bariopyrochlore	bariomicrolite	
	Species named by most abunda	REE*	yttropyrochlore ceriopyrochlore		yttrobetafite
	A-atom, other than Na or Ca	Pb	plumbopyrochlore	plumbomicrolite	plumbobetafite
		Bi		bismutomicrolite	
		U	uranopyrochlore	uranmicrolite	betafite

*REE = Y + (lanthanides), and for the purposes of species definition, REE counts as one *A*-atom
yttro = Y + (Gd → Lu), cerio = La → Eu.

Pyrochlore group minerals occur dominantly within carbonatites and rare-metal enriched granites and are refractory cubic oxide minerals. Whereas there are numerous studies of pyrochlore (mainly from carbonatites) and microlite (from rare-earth enriched granites and pegmatites) (e.g., Lumpkin *et al*., 1986; Ohnenstetter and Piantone, 1992; Wall *et al*., 1996; Tindle and Breaks, 1998), there is a paucity of geochemical data on betafite composition and no data from the Rössing area in the literature. Betafite contains significant uranium within the A-site and most analytical data available in the literature has been from metamict grains, although Mazzi and Munno (1983) presented two analyses of crystalline calciobetafite from an Italian sanidinite.

The occurrences of betafite/pyrochlore at Rössing have enabled further investigations of their crystal chemistry. The aim of this paper is to present geochemical analyses of betafite and pyrochlore from the Rössing area including rare-earth element data for betafite. It suggests possible factors that may control betafite formation and contributes to the discussion on the nature of the betafite alteration.

GEOLOGICAL SETTING

The Rössing Uranium Mine and adjacent prospects are situated in the Namib Desert approximately 65 km northeast of Swakopmund. They occur within the southern Central Zone of the NE-trending inland branch of the Damara Orogen. The Main Pit is termed the SJ area while other sub-economic occurrences of uranium mineralisation include the SH area to the west of the pit and the SK area to the east of the pit (Fig. 3). Uranium mineralisation is associated with intrusions of sheeted leucogranites, locally termed alaskites. These are emplaced into Neoproterozoic pelitic and calc-silicate country rocks of the Khan and Rössing Formations (Fig. 4). The intrusive leucogranite sheets are highly variable in texture; ranging from granophyric, aplitic and fine-, medium-, or coarse-grained granitic to pegmatitic. In size, the sheets vary from a few centimetres in width to more than a 100 m across and the larger sheets tend to show mineralogical banding. There is a range in colour from white, through cream, to grey or pink. Mineralogically, they consist essentially of quartz and feldspar, which may be a combination of microcline, perthite, albite or oligoclase. According to Herd (1996) modal compositions are dominantly within the monzogranite field of the IUGS QAP modal classification scheme of Le Bas and Streckeisen (1991). Whole-rock XRF analyses show that the granitic sheets are predominantly metaluminous, with a high silica content (Herd, 1996). Basson (pers. com.) has shown that the majority of leucogranite intrusions in the Rössing area are post D3 and equate to uranium-enriched types D and E of Nex *et al*. (2001) defined from the Goanikontes area some 30 km to the southwest.

The Rössing Mine is the only world producer of primary uranium from mineralised sheeted leucogranites. The ratio of primary to secondary minerals is approximately 1:1. The primary minerals are uraninite and pyrochlore/betafite, although the pyrochlore group minerals account for <5% of the uranium mineralisation within the main pit (SJ area). Secondary minerals are dominantly betauranophane/uranophane with metatorbernite, metahaweeite, carnotite, thorogummite and gummite (Von Backström, 1970). The secondary minerals are not confined to the leucogranite sheets, but are also present within cracks and joints of the surrounding metasediments. Berning (1986) provided a full account of the discovery and development of the mine. Beyond the environs of the mine, betafite comprises a significant proportion of the uranium mineralisation, particularly in the SH area, and in some localities is the only uranium-bearing mineral.

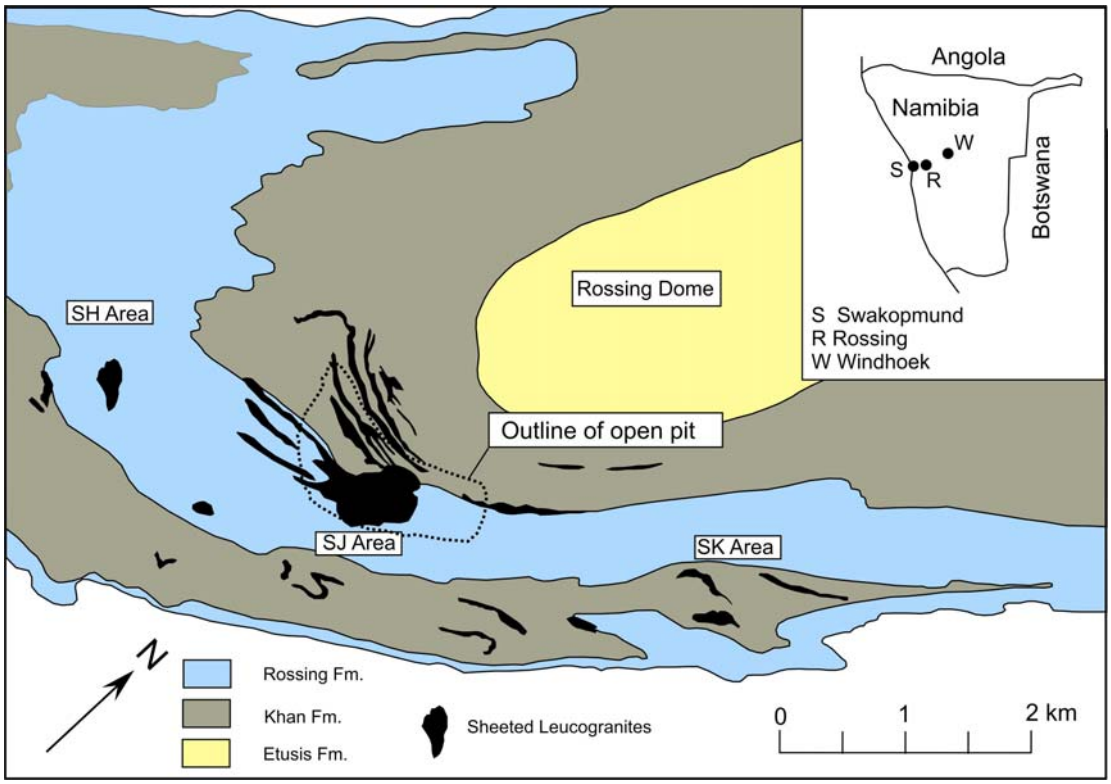

Figure 3: *Map showing the simplified geology of the Rössing area (after Smith, 1965) and the locations of the SJ pit, SH and SK uranium anomalies. Inset shows the location of Rossing Mine within Namibia.*

OCCURRENCE

Betafite/pyrochlore is found dominantly in the microcline-perthite facies of the leucogranites, often within quartz or at the contact between quartz and feldspar grains. Crystals of pyrochlore (ss) composition were only found in samples from the main Rössing pit. These occur as isolated honey-coloured crystals in a medium-grained, white leucogranite interbanded with amphibolite. Betafite occurs as a common accessory in the leucogranite of the SH area west of the Rössing Mine and in the SK area east of the mine (Fig. 3). It is rarely found in the Rössing Main Pit and is locally concentrated as a heavy mineral in recent stream sediments. Betafite occurs as small octahedra to subrounded, isolated, dodecahedral crystals or clusters of crystals up to 2 cm in size, although commonly of 1-3 mm diameter (Fig. 5a). Although betafite can occur in all the different granitic textures, it is most commonly observed in the medium-grained facies. Typically, betafite is greenish brown or yellowish brown in colour, although it shows a range from yellowish- or greenish-brown through grey to progressively darker colours, such as reddish brown or almost black body colour.

The presence of betafite is characterised by dark smoky quartz and a distinctive halo of radial cracks around the mineral (Fig. 5b). The quartz and feldspar in immediate contact with the betafite are often fractured (possibly due to expansion during metamictization), and this zone is permeated with red or yellow staining caused by the presence of various secondary uranium-, iron- and titanium-bearing minerals. In the SH and SJ areas, although accessory minerals that accompany betafite are sparse, they are very varied and include biotite, zircon, apatite, monazite, sphene and iron oxides. In the SK area to the east of the main mine (Fig. 1), the betafite is associated with allanite, biotite and radiating 'feather

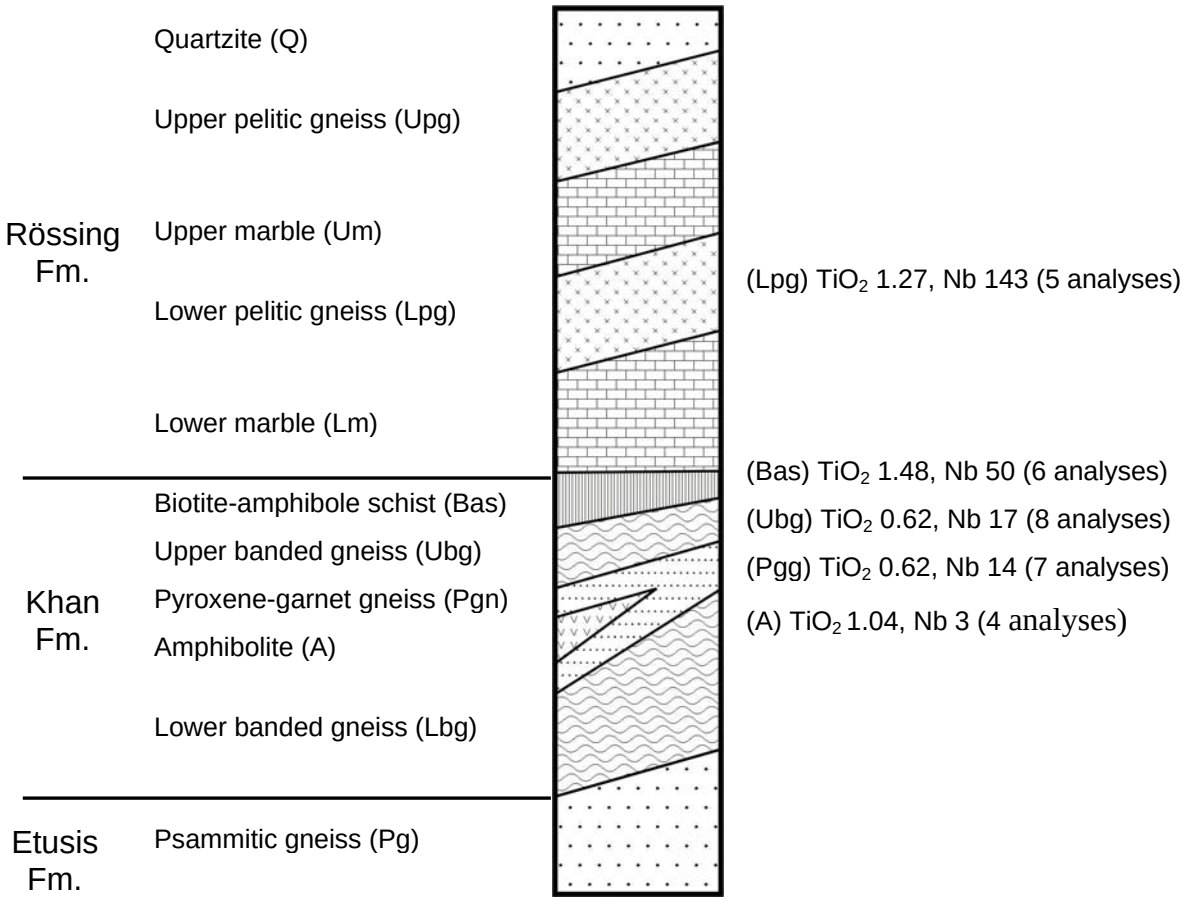

Figure 4: *Stratigraphic column of the Damara Sequence in the area of the Rössing Mine. TiO_2 and Nb contents for selected lithologies are shown, which are averages from a number of whole rock XRF analyses given by Herd (1996) and Nex (1997).*

growth' laths of alkali feldspar. In rare cases where betafite and uraninite have been observed in the same sample, the textural relationship between the two minerals suggest that uraninite occurred first, as it is present as an inclusion within a crystal of pyrochlore (Ixer, pers. comm.).

No mineralogical or textural features were found within the sheeted leucogranites that could be identified as a control on betafite occurrence. There is no apparent difference in the composition or abundance of feldspar, or in the proportions of quartz and feldspar in betafite-bearing or betafite-absent granitic sheets. In contrast, the country rocks may exert an effect on betafite formation. Betafite is frequently found where sheeted leucogranites cross-cut particular metasediments. Amphibole schist, and amphibolite of the Khan Formation, and cordierite gneisses of the Rössing Formation contain relatively high Ti and Nb that may contribute to the formation of betafite (Fig. 4). However, this cannot be the only control, otherwise betafite would be more abundant in the SJ Main Pit where sheeted leucogranites cut amphibole schist and amphibolite.

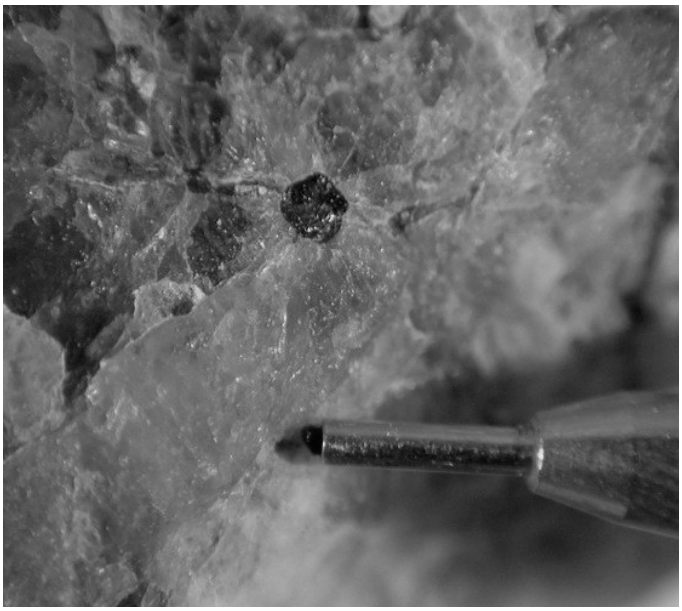

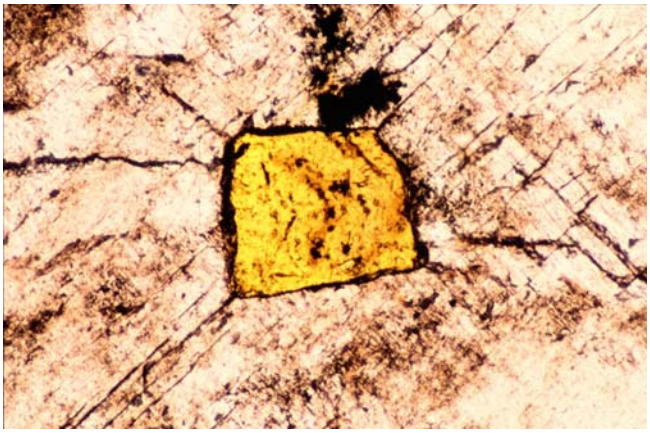

Figure 5: *(a) Glassy euhedral betafite grain with radial cracks within a medium-grained sheeted leucogranite with dark quartz. Width of pencil lead is 0.3 mm. (b) Plane-polarised light photomicrograph of betafite in thin section showing radial cracks in quartz host. Field of view is 2 mm.*

Betafite-bearing leucogranites appear to occur preferentially in the cores of antiformal structures where it is envisaged that the associated fluid did not escape, but was more readily retained to react with the leucogranite in the subsolidus. There may thus be a structural factor which influences betafite occurrence as the mineral occurs in locations where leucogranites invaded the cores of antiformal structures, or where they invaded amphibolite so that the fluid could not escape, or where thick overlying marbles inhibited fluid loss. There is therefore no simple single factor that controls betafite crystallisation. Rather there appears to be a combination of host-rock chemistry, fluid chemistry and structural factors that combine to favour betafite crystallisation.

The major difference between betafite-bearing and uraninite-bearing areas has come from a study on trapped fluids. A comparison of fluid compositional characteristics between the SH

area to the west where betafite is the dominant uranium-bearing phase and the main pit, where betafite is rare and uraninite is the main primary phase, was undertaken by fluid extraction analysis on a vacuum extraction train (Herd, 1996; Nex *et al*., 2002). Uraninite-bearing samples from the pit showed a total fluid content in excess of 10 micromoles per gram and typically 20-40 micromoles per gram, whereas fluid content in betafite-bearing SH samples was consistently low, typically 3-5 micromoles per gram. Absolute values of CO_2 show little difference between the pit and SH areas (typically 1-2 micromoles per gram). However, since the SH samples contain much lower amounts of water, the CO_2:H_2O ratio is much higher. This high CO_2 activity has clearly been important in influencing betafite crystallisation, which might be anticipated since pyrochlore group minerals are typical in alkaline rocks and carbonatites that are high in CO_2. Mitchell and Kjarsgaard (2003) have shown that water-bearing, fluorine-free melts are more likely to crystallise perovskite-structured minerals rather than pyrochlore and so it may be expected that high CO_2 will promote pyrochlore crystallisation.

SAMPLE PREPARATION

Betafite samples were collected from bulk samples of leucogranites from the SH and SJ areas, where betafite was evident on the weathered surface of the granite, and from radioactive concentrates in fluvial sands (SK and SH areas). Pyrochlore and betafite grains were separated from crushed bulk samples of SJ and SH area rocks, selected after whole-rock XRF analyses showed high Nb contents (> 100 ppm Nb). Mineral grains were separated by a combination of magnetic separation, heavy liquids, and hand-picking under a binocular microscope. Yellow and brown betafite from the SK area were separated from recent fluvial sands by hand-picking with a binocular microscope. Other betafites from bulk rock samples were dominantly brown/black in colour and could not be further differentiated. All samples were obtained from heavy mineral separates and details of analysis are shown in Table 2.

Table 2: Summary of sample details

Sample No	Source	Mineral	Analytical Method
90-1	SJ (Main Pit) at contact with amphibolite	Composite pyrochlore	EMP
90-2	SJ (Main Pit) 1.6 m from contact with amphibolite	Composite pyrochlore	EMP
90-4	SJ (Main Pit) 3 m from contact with amphibolite	Composite pyrochlore	EMP
90-24A	SJ (Main Pit) from thin SLG within amphibolite	Betafite	EMP
SH8A	SH area close to centre of leucogranite plug	Betafite	REE
SH8A	SH area close to centre of leucogranite plug	Apatite	REE
SH19	SH area close to centre of leucogranite plug	Betafite	EMP
SK Yellow	SK area fluvial sands	Betafite	XRF EMP
SK Brown	SK area fluvial sands	Betafite	XRF EMP

X-RAY POWDER DIFFRACTOMETRY

Betafite in the Rössing area contains substantial amounts of uranium, which renders it metamict. XRD investigations showed that the lattice damage affects the diffraction characteristics, commonly with the complete loss of characteristic peaks on XRD patterns. Following Ewing and Ehlmann (1975), Chakhmouradian and Mitchell, (1998) and others, analyses of grains after heating to 550°C revealed patterns and D-spacings compatible to

those of betafite. This suggests that on heating there is almost a complete restoration of the lattice and its diffraction characteristics.

COMPOSITIONAL VARIATIONS OF THE PYROCHLORE GROUP MINERALS

The chemical variation and zonation of the pyrochlore and betafite was studied using back-scattered electron (BSE) images, which depict differences in the mean atomic number at the surface of the sample. BSE images of pyrochlore grains from the main pit show significant within-grain variation (Figs. 6a and b), while betafite is much more homogeneous (Fig. 6c).

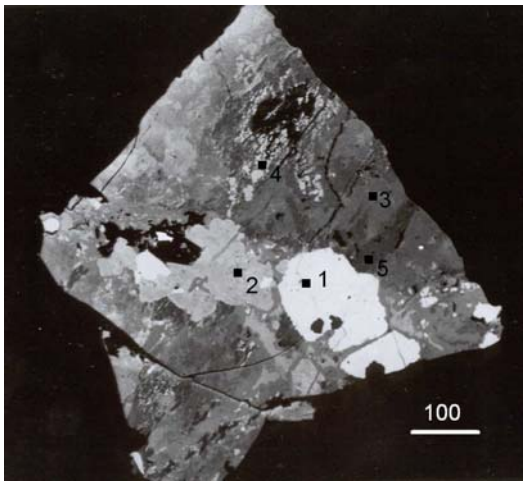

Figure 6a. *Backscatter electron photomicrograph of a composite pyrochlore grain, sample 90-1. The numbered spots show the locations of specific analyses detailed in Table 3. This grain contains at least three separate mineral phases: uranothorite (1); betafite (2); and pyrochlore (3-5).*

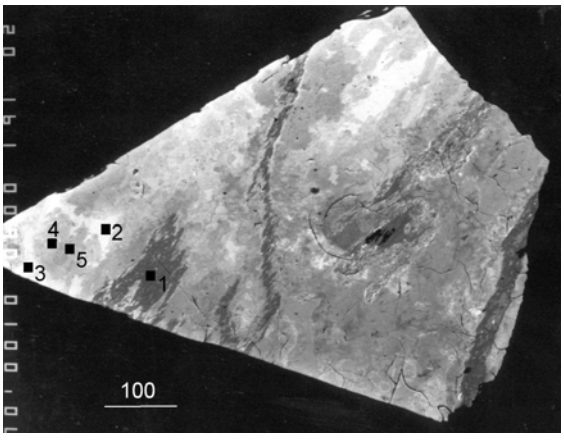

Figure 6b. *Backscatter electron photomicrograph of a composite pyrochlore grain, sample 90-2. The numbered spots show the locations of specific analyses detailed in Table 3. Although compositional variation is noted within the BSE image all analyses are of pyrochlore ss*.

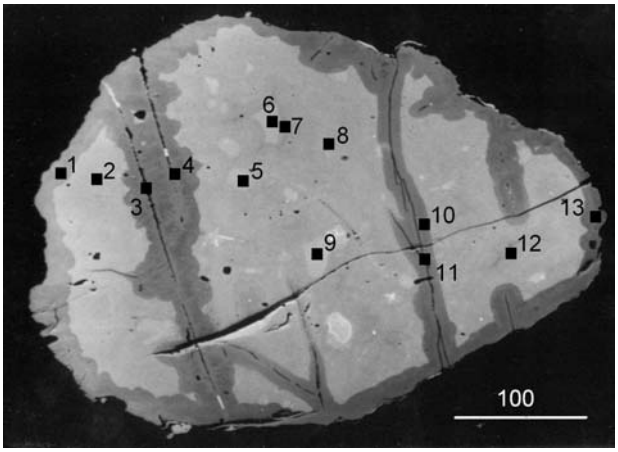

Figure 6c. *Backscatter electron photomicrograph of a betafite grain, sample 90-24A. The numbered spots show the locations of specific analyses detailed in Table 3. The dark bands cutting across the betafite grain correlate with fluid inclusion trails within the host quartz.*

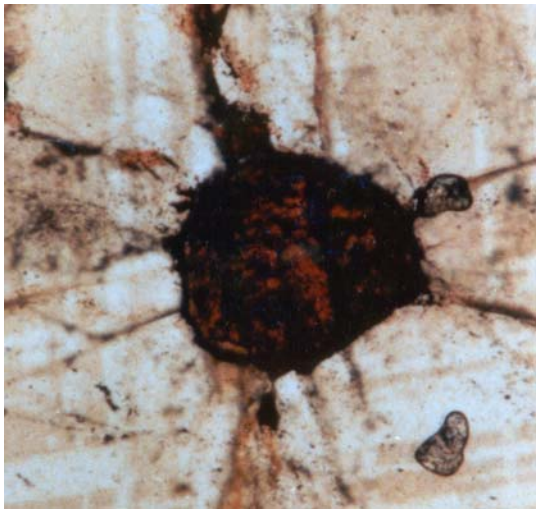

Figure 6d. *PPL photomicrograph of the same betafite grain in Figure 6c showing fluid inclusions trails which are continuous through the quartz host and the betafite grain.*

Electron microprobe analyses (EMPA) in Table 3 were carried out on samples of pyrochlore and betafite from the Rössing area, including those shown in Figure 6. These analyses were undertaken on a JEOL Superprobe JCXZ-733 in the Geology Department at the University of St-Andrews, Scotland. The operating conditions used were an accelerating voltage of 20 Kv and a beam current of 30 nA, with metal and natural mineral standards. REE analyses by EMPA (typically < 2wt % total REE) were later shown to be unreliable. LA-ICPMS analyses of REE gave REE contents of betafite and pyrochlore between 2-12 wt% (see below). Furthermore, the LA-ICPMS data showed typical REE patterns when normalised to chrondritic values, whereas EMPA REE analyses produced irregular chondrite-normalised REE patterns. Data obtained from EMPA were recalculated, omitting the REE data, following the method of Lumpkin *et al*. (1986) and Ohnenstetter and Piantone (1992) on the basis of 6 oxygen atoms

Note: Following page (pg. 10) in A3 landscape format.

Table 3: Electronprobe microanalysis of betafite and pyrochlore. REE data from the EMP were found to be unreliable (see LA-ICPMS data below) and were omitted from calculations to obtain cation and atomic percentage data.

Table 3: Electronprobe microanalysis of betafite and pyrochlore. REE data from the EMP were found to be unreliable (see LA-ICPMS data below) and were omitted from calculations to obtain cation and atomic percentage data

Sample	SK	SK	SH 19	SH 19	SH 19	SH 19	90-24A	90-24A	90-24A	90-24A	90-24A	90-24A	90-24A	90-24A	90-24A	90-24A	90-24A	90-24A	90-24A	90-1	90-1	90-1	90-1	90-1	90-2	90-2	90-2	90-2	90-2	90-4	90-4	90-4	90-4	90-4	90-4
	Bet	Bet	Bet	Bet	Bet	Bet	Bet	Bet	Bet	Bet	Bet	Bet	Bet	Bet	Bet	Bet	Bet	Bet	Bet	Urt	Bet	Py	Py	Py	Py	Py	Py	Py	Py	Py	Py	Urt	Lian	Py	Py	U-Nb-Y?
Analysis	Brown	Yellow	1	2	3	4	1	2	3	4	5	6	7	8	9	10	11	12	13	1	2	3	4	5	1	2	3	4	5	1	2	3	4	5	6
SiO2	n.d.	0.30	3.38	2.24	2.25	2.27	1.64	1.62	1.67	4.55	1.80	0.34	2.71	1.92	1.40	1.78	7.16	2.46	2.88	17.84	2.69	3.89	2.67	1.61	1.36	n.d.	n.d.	0.00	2.21	1.07	17.93	n.d.	0.12	0.79	5.21
FeO	1.16	0.54	1.47	0.68	0.75	0.67	0.75	0.65	0.61	0.64	0.72	0.74	0.51	0.80	0.70	0.80	0.72	0.53	0.83	0.13	1.44	1.02	0.96	0.95	1.30	7.75	3.78	3.28	5.28	0.67	0.16	0.03	1.52	0.92	0.71
MnO	0.09	n.d.	0.10	0.14	0.11	0.15	0.41	0.43	0.47	0.45	0.39	0.83	0.38	0.40	0.34	0.40	0.34	0.38	0.41	0.04	0.14	0.11	0.12	0.15	0.29	1.84	1.43	0.29	0.24	0.17	0.02	n.d.	0.05	0.12	0.09
CaO	12.79	3.36	3.78	3.05	3.15	3.07	8.64	9.06	10.54	8.37	7.46	12.19	8.34	8.30	6.83	8.99	10.99	8.25	8.29	1.70	4.97	5.16	5.62	9.76	11.58	0.60	0.37	3.32	3.76	4.49	1.57	0.17	5.74	12.88	2.90
Na2O	1.03	0.36	n.d.	0.69	0.52	0.60	0.07	0.44	0.32	0.36	0.29	0.89	0.27	0.33	0.30	0.08	0.40	0.46	0.60	0.16	0.15	0.26	0.30	0.27	n.d.	0.28	n.d.	0.51	n.d.	0.31	0.21	0.70	0.40	n.d.	0.55
K2O	n.d.	n.d.	0.69	0.43	0.09	0.37	n.d.	n.d.	n.d.	n.d.	n.d.	n.d.	n.d.	n.d.	n.d.	n.d.	n.d.	n.d.	n.d.	0.37	n.d.	0.10	n.d.	n.d.	n.d.	n.d.	n.d.	n.d.	0.10	n.d.	n.d.	n.d.	n.d.	n.d.	n.d.
Y2O3	0.59	0.29	n.d.	0.51	0.41	0.44	1.64	1.75	1.80	2.81	1.95	1.64	1.87	1.98	1.93	1.52	1.80	2.19	2.78	1.58	3.53	3.69	0.36	1.97	2.46	6.64	6.15	5.43	11.30	0.06	1.15	3.17	0.24	2.05	7.14
La2O3	0.22	n.d.	0.24	0.15	0.13	0.19	0.09	0.05	0.07	0.13	0.16	0.19	0.07	0.07	0.10	0.16	0.15	0.18	0.12	0.13	0.03	0.00	n.d.	n.d.	n.d.	n.d.	n.d.	0.02	0.08	n.d.	n.d.	0.07	n.d.	0.01	n.d.
Ce2O3	0.90	0.35	0.46	0.92	0.84	0.92	1.21	1.24	1.29	0.90	1.22	1.14	1.23	1.10	1.26	1.08	0.83	1.36	1.21	n.d.	0.26	0.26	0.14	n.d.	n.d.	0.43	0.55	0.38	0.31	0.04	n.d.	n.d.	n.d.	0.05	0.04
Pr2O3	0.15	n.d.	0.04	0.07	0.14	0.03	0.19	0.13	0.19	0.17	0.17	0.17	0.18	0.13	0.18	0.10	0.15	0.04	0.18	0.06	n.d	0.08	n.d.	n.d.	0.05	0.14	0.03	0.00	0.11	n.d.	0.02	n.d.	0.07	n.d.	0.03
Nd2O3	0.45	0.23	0.07	0.42	0.32	0.41	0.63	0.68	0.64	0.54	0.74	0.68	0.69	0.75	0.82	0.59	0.51	0.67	0.58	n.d.	n.d	0.45	n.d.	n.d.	0.14	0.29	0.43	0.40	0.34	n.d.	0.02	0.06	0.08	n.d.	0.07
Sm2O3	0.04	n.d.	0.09	0.04	0.11	0.11	0.20	0.23	0.22	0.13	0.17	0.21	0.15	0.22	0.06	0.12	0.13	0.15	0.15	0.02	0.03	0.18	n.d.	0.14	0.06	0.27	0.25	0.16	0.21	0.03	n.d.	0.07	n.d.	0.06	0.20
Gd2O3	0.01	n.d.	n.d.	n.d.	n.d.	n.d.	0.19	0.14	0.14	n.d.	0.16	0.14	0.06	n.d.	0.07	0.13	0.16	0.16	0.06	0.00	n.d	0.58	n.d.	0.35	0.38	0.72	0.67	0.72	1.09	n.d.	0.02	0.12	0.01	0.44	0.85
Dy2O3	0.13	n.d.	n.d.	0.15	0.11	0.11	0.25	0.18	0.30	0.04	0.30	0.36	0.25	0.24	0.28	0.30	0.26	0.25	0.23	0.25	0.29	0.95	n.d.	0.41	0.38	0.91	0.87	1.02	1.69	0.10	0.15	0.38	0.04	0.41	1.66
Yb2O3	n.d	n.d.	0.04	0.05	0.04	0.11	0.33	0.36	0.21	0.17	0.36	0.29	0.38	0.35	0.36	0.41	0.26	0.34	0.36	0.22	0.48	0.94	0.22	0.47	0.74	1.62	1.61	1.32	2.20	0.06	0.12	0.36	0.03	0.73	3.39
ThO2	0.44	0.17	1.76	1.06	0.99	0.94	1.02	1.12	1.07	5.96	1.15	1.07	1.13	1.03	1.00	1.10	0.75	1.09	1.05	51.51	0.02	3.62	n.d.	0.80	0.98	3.55	3.57	3.96	2.84	0.01	55.68	10.33	0.42	0.84	3.78
UO2	27.55	30.36	48.22	29.16	29.34	28.51	27.67	27.93	28.46	29.90	28.17	27.14	28.26	27.57	27.17	26.43	27.93	28.17	28.05	17.79	24.60	9.26	20.83	4.52	4.63	17.53	20.17	19.34	7.44	25.88	19.63	79.68	0.19	3.43	26.86
PbO	1.29	1.55	1.10	1.77	1.28	1.23	1.32	1.50	2.34	1.70	1.73	1.87	0.89	2.19	4.82	2.04	2.35	0.86	1.25	n.d.	0.46	0.00	0.82	n.d.	n.d.	0.35	0.27	0.13	0.04	1.55	0.04	5.48	n.d.	n.d.	n.d.
W2O7	0.49	2.06	1.08	3.05	2.75	2.78	5.67	5.76	6.15	5.39	5.90	4.75	5.06	5.52	6.30	5.16	3.41	5.45	5.88	n.d.	n.d.	0.00	n.d.	n.d.	n.d.	2.38	2.83	1.11	1.31	n.d.	n.d.	n.d.	0.01	n.d.	n.d.
ZrO2	0.04	n.d.	0.13	0.04	0.08	0.08	0.02	0.13	0.03	n.d.	0.05	0.03	0.10	0.08	0.01	n.d.	0.01	n.d.	n.d.	1.76	0.01	0.18	0.27	n.d.	0.04	0.53	0.51	0.48	0.28	0.16	0.06	n.d.	0.07	0.06	0.12
Nb2O5	24.52	28.96	14.06	22.85	23.03	22.57	20.21	20.72	21.10	18.47	21.49	20.03	21.09	20.49	20.65	20.44	21.85	20.58	19.88	0.22	19.53	49.08	25.28	62.32	67.42	43.49	46.57	45.09	42.68	22.78	0.44	0.10	79.09	65.22	34.85
Ta2O5	4.41	6.00	2.22	2.98	3.15	3.38	3.32	3.22	3.09	2.65	3.14	3.16	3.20	3.06	3.05	3.05	3.09	3.22	3.92	0.07	23.96	8.77	30.93	7.22	7.27	6.26	6.26	6.02	7.27	31.93	0.10	0.45	0.68	7.56	6.84
TiO2	19.23	17.46	19.78	21.62	21.53	20.98	23.11	23.81	23.51	20.02	24.17	22.98	24.16	23.39	23.10	23.32	18.37	24.10	23.62	n.d	11.11	1.18	5.89	1.34	1.32	0.75	0.75	0.71	1.26	10.33	n.d.	n.d.	0.50	1.42	0.47
Total	95.54	91.99	98.71	92.07	91.12	89.92	98.58	101.15	104.22	103.35	101.69	100.84	100.98	99.92	100.73	98.00	101.62	100.89	102.33	93.85	93.69	89.77	94.41	92.28	100.39	96.34	97.07	96.36	92.03	99.61	97.30	101.16	89.24	96.98	95.73
Si	0.0000	0.0210	0.3049	0.1590	0.1596	0.1643	0.1137	0.1093	0.1128	0.3572	0.1190	0.0239	0.1813	0.1319	0.0962	0.1232	0.5640	0.1658	0.1967	~~~	0.2269	0.3048	0.2188	0.1034	0.0810	0.0000	0.0000	0.2322	0.1946	0.0798	~~~	~~~	0.0068	0.0485	0.5781
Fe	0.0721	0.0318	0.1109	0.0404	0.0445	0.0406	0.0435	0.0367	0.0345	0.0420	0.0398	0.0436	0.0285	0.0460	0.0402	0.0463	0.0474	0.0299	0.0474	~~~	0.1013	0.0668	0.0658	0.0510	0.0651	0.5692	0.2602	0.2376	0.3891	0.0418	~~~	~~~	0.0697	0.0471	0.0654
Mn	0.0054	0.0000	0.0076	0.0084	0.0066	0.0092	0.0241	0.0246	0.0269	0.0299	0.0218	0.0495	0.0215	0.0233	0.0198	0.0234	0.0227	0.0217	0.0237	~~~	0.0103	0.0070	0.0083	0.0082	0.0144	0.1371	0.1000	0.0215	0.0176	0.0105	~~~	~~~	0.0025	0.0062	0.0081
Ca	1.0195	0.2538	0.3654	0.2319	0.2395	0.2380	0.6418	0.6547	0.7627	0.7040	0.5285	0.9197	0.5979	0.6110	0.5026	0.6666	0.9275	0.5959	0.6065	~~~	0.4494	0.4330	0.4935	0.6715	0.7413	0.0566	0.0323	0.3084	0.3555	0.3584	~~~	~~~	0.3383	0.8454	0.3442
Na	0.1488	0.0492	0.0000	0.0949	0.0715	0.0842	0.0094	0.0575	0.0419	0.0548	0.0372	0.1215	0.0350	0.0440	0.0399	0.0107	0.0611	0.0601	0.0794	~~~	0.0245	0.0401	0.0477	0.0336	0.0000	0.0473	0.0000	0.0854	0.0000	0.0445	~~~	~~~	0.0421	0.0000	0.1172
K	0.0000	0.0000	0.0794	0.0389	0.0081	0.0342	0.0000	0.0000	0.0000	0.0000	0.0000	0.0000	0.0000	0.0000	0.0000	0.0000	0.0000	0.0000	0.0000	~~~	0.0000	0.0100	0.0000	0.0000	0.0000	0.0000	0.0000	0.0000	0.0111	0.0000	~~~	~~~	0.0000	0.0000	0.0000
Y	0.0234	0.0109	0.0000	0.0192	0.0155	0.0169	0.0604	0.0627	0.0646	0.1173	0.0685	0.0614	0.0665	0.0723	0.0705	0.0559	0.0754	0.0785	0.1009	~~~	0.1583	0.1534	0.0157	0.0673	0.0780	0.3101	0.2692	0.2502	0.5299	0.0023	~~~	~~~	0.0070	0.0668	0.4209
La	0.0061	0.0000	0.0080	0.0039	0.0034	0.0051	0.0023	0.0012	0.0017	0.0038	0.0039	0.0049	0.0017	0.0018	0.0025	0.0041	0.0044	0.0045	0.0030	~~~	0.0008	0.0000	0.0000	0.0000	0.0000	0.0000	0.0000	0.0005	0.0025	0.0000	~~~	~~~	0.0000	0.0001	0.0000
Ce	0.0245	0.0090	0.0152	0.0239	0.0218	0.0244	0.0307	0.0306	0.0319	0.0258	0.0295	0.0294	0.0301	0.0276	0.0317	0.0273	0.0239	0.0335	0.0302	~~~	0.0079	0.0074	0.0042	0.0000	0.0000	0.0138	0.0167	0.0119	0.0099	0.0010	~~~	~~~	0.0000	0.0010	0.0017
Th	0.0074	0.0027	0.0361	0.0171	0.0160	0.0155	0.0161	0.0172	0.0164	0.1065	0.0173	0.0171	0.0172	0.0161	0.0156	0.0173	0.0134	0.0167	0.0163	~~~	0.0003	0.0644	0.0000	0.0117	0.0133	0.0709	0.0670	0.0782	0.0571	0.0002	~~~	~~~	0.0052	0.0117	0.0955
U	0.4560	0.4762	0.9680	0.4605	0.4632	0.4591	0.4268	0.4191	0.4277	0.5223	0.4145	0.4253	0.4208	0.4215	0.4152	0.4070	0.4895	0.4225	0.4262	~~~	0.4617	0.1613	0.3799	0.0646	0.0616	0.3425	0.3698	0.3731	0.1459	0.4293	~~~	~~~	0.0024	0.0468	0.6629
Pb	0.0259	0.0294	0.0267	0.0338	0.0245	0.0240	0.0246	0.0272	0.0425	0.0359	0.0308	0.0355	0.0160	0.0405	0.0891	0.0380	0.0498	0.0156	0.0230	~~~	0.0104	0.0000	0.0181	0.0000	0.0000	0.0083	0.0059	0.0029	0.0009	0.0311	~~~	~~~	0.0000	0.0000	0.0000
W	0.0092	0.0364	0.0244	0.0542	0.0489	0.0504	0.0985	0.0973	0.1040	0.1060	0.0977	0.0838	0.0848	0.0950	0.1084	0.0895	0.0673	0.0920	0.1006	~~~	0.0000	0.0000	0.0000	0.0000	0.0000	0.0524	0.0583	0.0242	0.0290	0.0000	~~~	~~~	0.0001	0.0000	0.0000
Zr	0.0014	0.0000	0.0057	0.0014	0.0028	0.0028	0.0007	0.0043	0.0010	0.0000	0.0016	0.0010	0.0033	0.0027	0.0003	0.0000	0.0004	0.0000	0.0000	~~~	0.0005	0.0068	0.0108	0.0000	0.0012	0.0229	0.0205	0.0205	0.0120	0.0057	~~~	~~~	0.0020	0.0018	0.0065
Nb	0.8246	0.9230	0.5735	0.7331	0.7388	0.7384	0.6334	0.6318	0.6442	0.6555	0.6424	0.6377	0.6380	0.6365	0.6412	0.6395	0.7781	0.6272	0.6137	~~~	0.7449	1.7369	0.9368	1.8092	1.8211	1.7261	1.7347	1.7671	1.7014	0.7678	~~~	~~~	1.9670	1.8068	1.7476
Ta	0.0893	0.1150	0.0545	0.0575	0.0608	0.0665	0.0626	0.0591	0.0567	0.0566	0.0565	0.0605	0.0582	0.0572	0.0570	0.0574	0.0662	0.0590	0.0728	~~~	0.5497	0.1868	0.6894	0.1261	0.1182	0.1494	0.1403	0.1420	0.1743	0.6474	~~~	~~~	0.0101	0.1260	0.2063
Ti	1.0756	0.9256	1.3420	1.1538	1.1488	1.1418	1.2048	1.2076	1.1940	1.1819	1.2018	1.2170	1.2157	1.2086	1.1931	1.2136	1.0881	1.2217	1.2129	~~~	0.7050	0.0696	0.3630	0.0647	0.0595	0.0492	0.0462	0.0463	0.0834	0.5791	~~~	~~~	0.0208	0.0654	0.0395

Sample	SK	SK	SH 19	SH 19	SH 19	SH 19	90-24A	90-24A	90-24A	90-24A	90-24A	90-24A	90-24A	90-24A	90-24A	90-24A	90-24A	90-24A	90-24A	90-1	90-1	90-1	90-1	90-2	90-2	90-2	90-2	90-2	90-4	90-4	90-4	90-4
Analysis	Brown	Yellow	1	2	3	4	1	2	3	4	5	6	7	8	9	10	11	12	13	2	3	4	5	1	2	3	4	5	1	4	5	6
Tot A	1.8	0.9	1.9	1.1	1.1	1.1	1.4	1.4	1.6	2.0	1.3	1.7	1.4	1.4	1.3	1.4	2.3	1.4	1.6	1.5	1.2	1.3	1.0	1.1	1.6	1.1	1.6	1.7	1.0	0.5	1.1	2.3
Ca at%	57.0	28.7	19.0	20.5	22.3	21.3	46.1	45.4	48.8	35.2	40.3	53.1	42.2	42.5	38.0	46.9	40.7	41.2	39.0	31.0	34.7	39.4	66.4	70.3	3.6	2.9	19.2	20.7	35.9	71.4	78.7	15.0
Na at%	8.3	5.6	0.0	8.4	6.7	7.5	0.7	4.0	2.7	2.7	2.8	7.0	2.5	3.1	3.0	0.8	2.7	4.2	5.1	1.7	3.2	3.8	3.3	0.0	3.0	0.0	5.3	0.0	4.5	8.9	0.0	5.1
K at%	0.0	0.0	4.1	3.4	0.8	3.1	0.0	0.0	0.0	0.0	0.0	0.0	0.0	0.0	0.0	0.0	0.0	0.0	0.0	0.0	0.8	0.0	0.0	0.0	0.0	0.0	0.0	0.6	0.0	0.0	0.0	0.0
Y at%	1.3	1.2	0.0	1.7	1.4	1.5	4.3	4.4	4.1	5.9	5.2	3.5	4.7	5.0	5.3	3.9	3.3	5.4	6.5	10.9	12.3	1.3	6.7	7.4	19.9	24.0	15.6	30.9	0.2	1.5	6.2	18.3
Ce at%	1.4	1.0	0.8	2.1	2.0	2.2	2.2	2.1	2.0	1.3	2.3	1.7	2.1	1.9	2.4	1.9	1.0	2.3	1.9	0.5	0.6	0.3	0.0	0.0	0.9	1.5	0.7	0.6	0.1	0.0	0.1	0.1
Pb at%	1.4	3.3	1.4	3.0	2.3	2.1	1.8	1.9	2.7	1.8	2.3	2.0	1.1	2.8	6.7	2.7	2.2	1.1	1.5	0.7	0.0	1.4	0.0	0.0	0.5	0.5	0.2	0.1	3.1	0.0	0.0	0.0
Si at%	0.0	2.4	15.9	14.0	14.9	14.7	8.2	7.6	7.2	17.9	9.1	1.4	12.8	9.2	7.3	8.7	24.7	11.5	12.7	15.6	24.4	17.5	10.2	7.7	0.0	0.0	14.5	11.4	8.0	1.4	4.5	25.2
Fe at%	4.0	3.6	5.8	3.6	4.1	3.6	3.1	2.5	2.2	2.1	3.0	2.5	2.0	3.2	3.0	3.3	2.1	2.1	3.1	7.0	5.4	5.3	5.0	6.2	36.6	23.2	14.8	22.7	4.2	14.7	4.4	2.9
Mn at%	0.3	0.0	0.4	0.7	0.6	0.8	1.7	1.7	1.7	1.5	1.7	2.9	1.5	1.6	1.5	1.7	1.0	1.5	1.5	0.7	0.6	0.7	0.8	1.4	8.8	8.9	1.3	1.0	1.0	0.5	0.6	0.4
Th at%	0.4	0.3	1.9	1.5	1.5	1.4	1.2	1.2	1.1	5.3	1.3	1.0	1.2	1.1	1.2	1.2	0.6	1.2	1.1	0.0	5.2	0.0	1.2	1.3	4.6	6.0	4.9	3.3	0.0	1.1	1.1	4.2
U at%	25.5	53.9	50.4	40.7	43.1	41.2	30.6	29.1	27.4	26.1	31.6	24.6	29.7	29.4	31.4	28.7	21.5	29.2	27.4	31.8	12.9	30.3	6.4	5.8	22.0	33.0	23.3	8.5	43.0	0.5	4.4	28.9
A-atom	1.8	0.9	1.9	1.1	1.1	1.1	1.4	1.4	1.6	2.0	1.3	1.7	1.4	1.4	1.3	1.4	2.3	1.4	1.6	1.5	1.2	1.3	1.0	1.1	1.6	1.1	1.4	1.7	1.0	0.5	1.1	2.3
B-atom	2.0	2.0	2.0	2.0	2.0	2.0	2.0	2.0	2.0	2.0	2.0	2.0	2.0	2.0	2.0	2.0	2.0	2.0	2.0	2.0	2.0	2.0	2.0	2.0	2.0	2.0	2.0	2.0	2.0	2.0	2.0	2.0
Tot B	2.0	2.0	2.0	2.0	2.0	2.0	2.0	2.0	2.0	2.0	2.0	2.0	2.0	2.0	2.0	2.0	2.0	2.0	2.0	2.0	2.0	2.0	2.0	2.0	2.0	2.0	2.0	2.0	2.0	2.0	2.0	2.0
W at%	0.5	1.8	1.2	2.7	2.4	2.5	4.9	4.9	5.2	5.3	4.9	4.2	4.2	4.8	5.4	4.5	3.4	4.6	5.0	0.0	0.0	0.0	0.0	0.0	2.6	2.9	1.2	1.5	0.0	0.0	0.0	0.0
Zr at%	0.1	0.0	0.3	0.1	0.1	0.1	0.0	0.2	0.0	0.0	0.1	0.1	0.2	0.1	0.0	0.0	0.0	0.0	0.0	0.0	0.3	0.5	0.0	0.1	1.1	1.0	1.0	0.6	0.3	0.1	0.1	0.3
Ti at%	53.8	46.3	67.1	57.7	57.4	57.1	60.2	60.4	59.7	59.1	60.1	60.8	60.8	60.4	59.7	60.7	54.4	61.1	60.6	35.3	3.5	18.2	3.2	3.0	2.5	2.3	2.3	4.2	29.0	1.0	3.3	2.0
Ta at%	4.5	5.8	2.7	2.9	3.0	3.3	3.1	3.0	2.8	2.8	2.8	3.0	2.9	2.9	2.8	2.9	3.3	3.0	3.6	27.5	9.3	34.5	6.3	5.9	7.5	7.0	7.1	8.7	32.4	0.5	6.3	10.3
Nb at%	41.2	46.1	28.7	36.7	36.9	36.9	31.7	31.6	32.2	32.8	32.1	31.9	31.9	31.8	32.1	32.0	38.9	31.4	30.7	37.2	86.8	46.8	90.5	91.1	86.3	86.7	88.4	85.1	38.4	98.4	90.3	87.4

and assuming that the sum of the cations (Nb + Ta + Ti + W + Zr) occupying the B-site is equal to 2. Fe has been assigned to the A-site, which assumes all Fe exists as Fe^{3+} following Williams *et al*. (1997) and Hogarth *et al*. (2000). EPMA results from all samples are shown in Table 3.

CATION VARIATION

Previously published analytical data for betafite indicates a large variation in cationic species in both A- and B-sites. There may also be considerable cation deficiency in the A-site for both betafite and pyrochlore with vacancy varying from 0.1 to 1 pfu. The betafite from Rössing is typical in this respect. Most betafite samples described prior to 1983 approached the AB_2O_6 stochiometry characteristic of many defect pyrochlores with <0.6 Ca, 0.1 Na, and 0.1 F atoms per formula unit (Lumpkin and Ewing, 1996). Calciobetafite from the type locality approaches ideal $A_2B_2O_7$ stoichiometry with 1.3 Ca, 0.2 Na and 0.3 F atoms pfu (Mazzi and Munno, 1983). A study of alteration effects by Lumpkin *et al*. (1988) and Lumpkin and Ewing, (1996) showed that alteration resulted in non-stoichiometry in betafite, with orange betafite showing the least alteration. Yellow and black-brown grains from Rössing also show distinct differences in A-site occupancy. Although the formula calculation requires that B-site occupancy sums to 2 cations, there is some variation in the cationic species occupying the B-site. In order to deal with this variation, A- and B- site cation variation are considered separately and the range and averages for individual B- and A-site cations are shown in Table 4.

B-site cation variation

Pyrochlore (ss) and betafite generally plot in distinct groups in their separate fields on the pyrochlore mineral discrimination diagram (Fig. 7). In betafite, the B-site is dominated by Ti and Nb with some variation, while most pyrochlore analyses are constrained to a small area of the graph towards the Nb end-member. Although brown betafite contains higher Ti than yellow betafite, the colour variation is probably defined more by A-site deficiency than Ti or Nb contents (see below). W is present in betafite and accounts for 0-5 at% while it is less abundant in pyrochlore at 0 to 2.6 at%. Zirconium is less abundant in betafite (0.0-0.3 at%) than in pyrochlore (0.0-1.1 at%). Two analyses from sample 90-1, which plot close to the pyrochlore-microlite-betafite boundaries (90-1,2 and 90-1,4) are from an inhomogeneous crystal of dominantly pyrochlore composition (Fig. 5a). Sample 90-1,2 is from a betafite inclusion within the pyrochlore. Analysis 90-4,1 is a high-Ta pyrochlore that also plots in a similar position.

A-site cation variation

In betafite, the principle cations occupying the A-site are Ca and U, whereas the A-site occupancy in pyrochlore is generally dominated by Ca although there are significant variations in Si, Fe, Y and U content (Tables 3 and 4). According to Gasperin (1960) full occupancy of the A-site is not essential for the stability of the pyrochlore structure. In pyrochlore the significant A-site cations are: Ca, Y, Si, Fe, Th, U, Pb, Mn and A-site occupancy varies from 0.47 to 1.71. In betafite the significant A-site cations are: Ca, Na, Y, Ce, Pb, Si, Fe, Mn, Th, and U with A-site occupancy varying from 0.88 to 2.28. A-site occupancy greater than 2.0 in two samples (90-24A(4) and 90-24A(11)), shown in Figure 5a, are both from alteration cracks within the betafite grain (Fig. 6c).

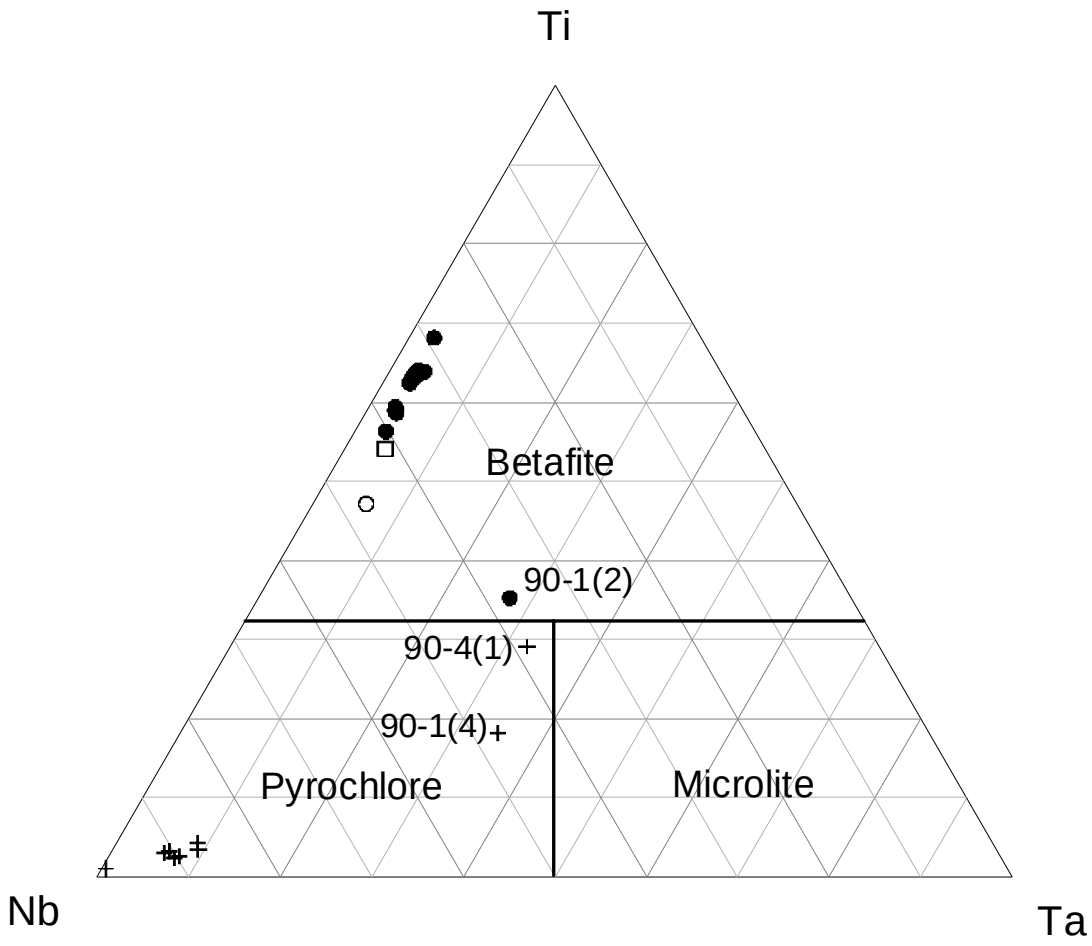

Figure 7. *Pyrochlore-group mineral discrimination diagram showing analyses from this study. The open square is brown betafite, open circle is yellow betafite, filled circles are betafite (undifferentiated) and crosses are pyrochlore analyses.*

Figure 8a shows that there is a marked difference in the A-site occupancy between brown betafite, which has close to full site occupancy and yellow betafite, which shows > 1 atom per formula unit (pfu) vacancy. All other analysed betafite have A-site occupancies between these two end-members. Pyrochlore shows a similar variation in A-site occupancy although having a greater variation in U pfu. In a study of microlite-pyrochlore Ohnenstetter and Piantone (1992) suggested that A-site vacancies were related to uranium content, but this is not the case for betafite from Rössing, which show a fairly uniform U content pfu (0.40-0.52). However, if uranium is portrayed as an atomic percentage then relatively higher proportions of U are associated with greater depletion of A-site cations (Fig. 8b).

Other A-site cations, which vary between the brown and yellow betafite end-members, include Ca and Na. Figure 9 shows that increasing A-site vacancies are related to depletion in Ca + Na. The presence of significant Si in three analysis (12-25 at%) from within the dark bands of sample 90-24A (Fig. 5c) is probably related to alteration. These analyses also show high levels of A-site occupancy (> 1.6).

Table 4: Range and averages for cation atomic % within pyrochlore and betafite. Analyses 90-1(2), 90-1(4), and 90-4(1) are not included in the data set

		pyrochlore		betafite	
	Cation	Range	Average	Range	Average
B-site cations	W	0 – 2.9	0.9	0.5 – 5.4	3.8
	Zr	0 – 1.1	0.5	0 – 0.3	0.1
	Ti	1.0 – 4.2	2.8	46.3 – 67.1	58.8
	Ta	0.5 – 9.3	6.5	2.7 – 5.7	3.2
	Nb	86.3 – 98.3	89.3	28.7 – 46.1	34.1
A-site cations	Ca	2.9 – 78.7	40.9	19.0 – 58.0	38.4
	Na	0 – 8.9	2.6	0 – 8.4	4.1
	K	0 – 0.8	0.2	0 – 4.1	0.6
	Y	1.5 – 30.9	13.8	0 – 5.9	3.6
	Ce	0 – 1.5	0.5	0.8 – 2.4	1.8
	Pb	0 – 0.5	0.1	1.1 – 6.7	2.3
	Si	0 – 24.4	8.2	0 – 24.7	10.5
	Fe	4.4 – 36.6	14.8	2.0 – 5.8	3.1
	Mn	0.5 – 8.9	2.7	0 – 2.9	1.3
	Th	1.1 – 6.0	3.2	0.3 – 5.3	1.3
	U	0.5 – 33.0	13.0	21.5 – 53.9	32.7

REE CHEMISTRY

Laser ablation ICP-MS analyses of single betafite crystals were undertaken on hand-picked yellow and brown grains from sample SH8A. The results are presented in Table 5 and Figure 10. REE contents of betafite are high, particularly the brown betafite, which can contain up to 14.5 wt%. Yellow betafite, however, is less variable in total REE content with a range of 1 - 3.5 wt%. The chondrite-normalised REE patterns exhibited by both brown and yellow betafite are generally flat with a negative Eu anomaly and minor depletion of La and less significantly Ce. Yellow betafite is slightly more depleted in LREE (La and Ce) compared to the brown variety.

DISCUSSION

According to Hogarth (1977), Ti-rich species of pyrochlore range from 33 to 55 % Ti, where Nb+Ta+Ti = 100%. He suggested further that analyses that report larger amounts of titanium may represent mixtures. However, as the analyses in Tables 3-4 show, titanium does exceed 55 atomic %Ti in many of the betafites from the Rössing area and is not due to mixtures since backscatter images and microprobe analyses confirm that most betafites do not contain other mineralogical phases. Even where pyrochlore group minerals are composite, the betafite phase is not a mixture with other Ti-bearing phases. The highest Ti atomic percentages coincide with lowest uranium contents in the mineral.

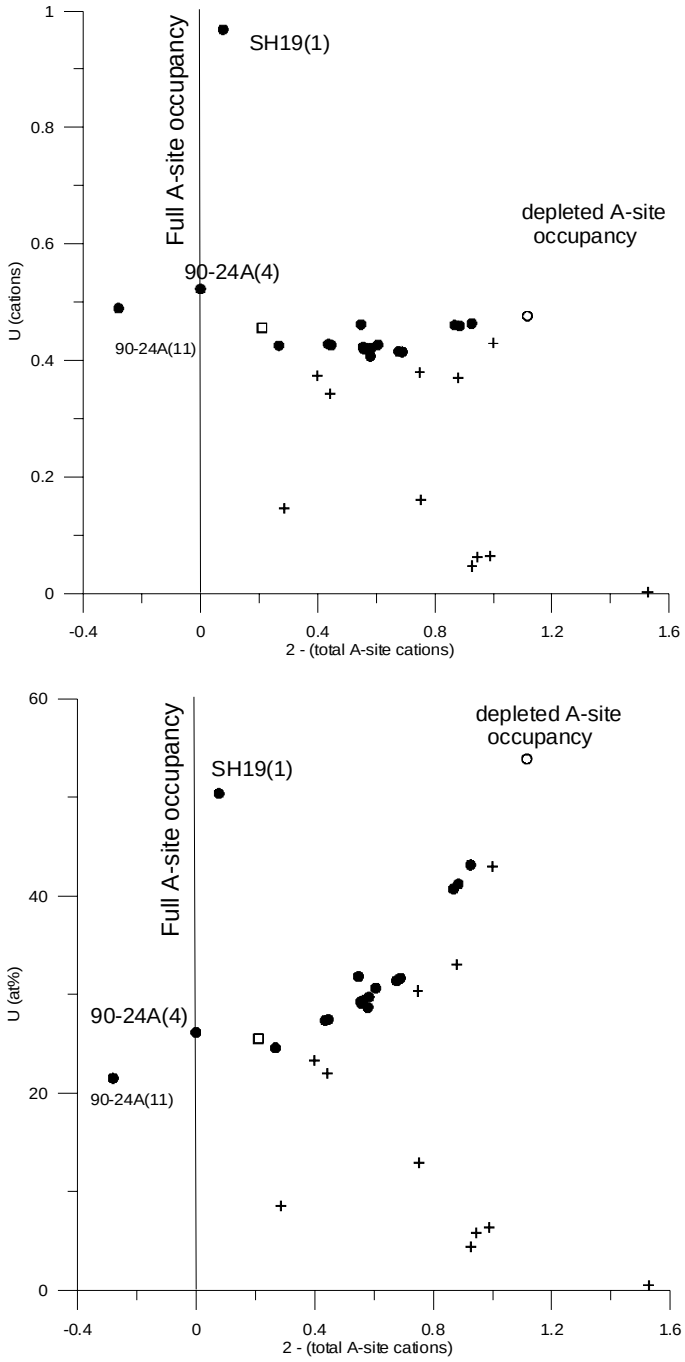

Figure 8. *Graphs showing: (a) A-site occupancy in pyrochlore and betafite and relatively constant U (cations) in betafite with varying concentrations in pyrochlore; and (b) A-site variation in betafite and pyrochlore relative to the cation percentagage of U. Symbols as in Figure 7.*

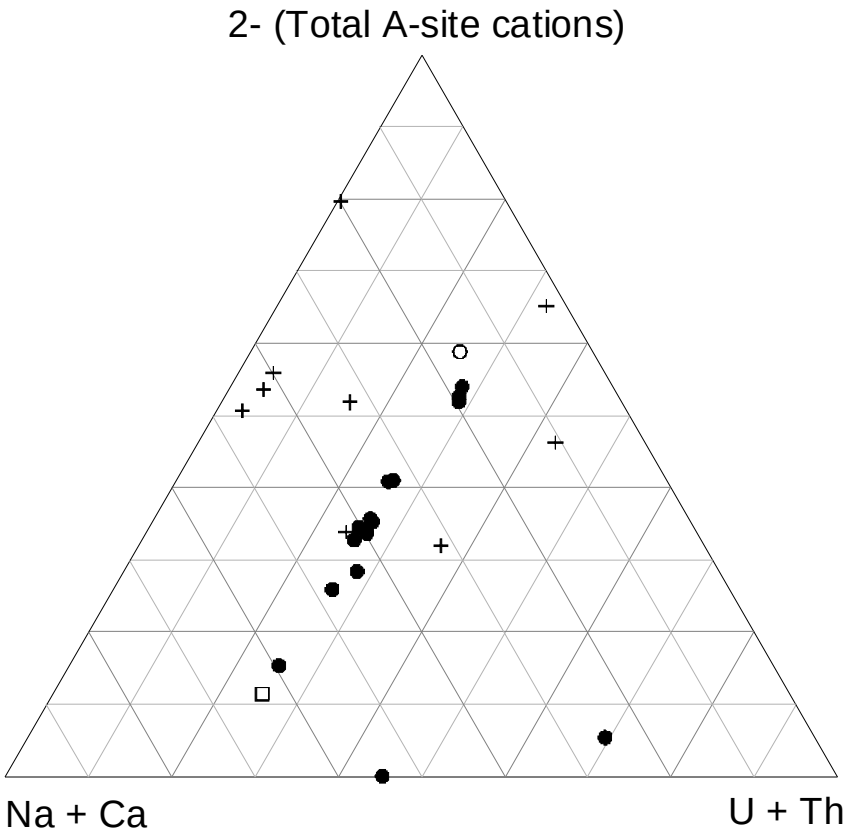

Figure 9. *Triangular diagram showing the variation in Na + Ca content in betafite and pyrochlore with A-site vacancies and the relatively constant U + Th content. Symbols as in Figure 7.*

SK brown betafite appears to be the most 'pristine'. It has the highest Ca and Na and lacks silica. The structural formula for this betafite, based on a B-site occupancy of 2, gives an A-site vacancy of <0.2 with 1 Ca and 0.15 Na pfu. Similar A-site occupancy is shown by sample 90-24A.6. Analysis SH 19.1 shows an A-site vacancy of only 0.1, but differs from the other two analyses with close to full A-site occupancy because Ca accounts for only 0.4 pfu of the A-site with U accounting for most of the site-filling (1 pfu).

In contrast, the SK yellow betafite has an A-site vacancy of 1.1, with 0.25 Ca, 0.05 Na and 0.02 Si pfu. All other analyses lie between the two end-members of the SK brown and SK yellow betafites. The yellow betafites appear therefore to be altered and to show an increase in silica and loss of Fe, Ti and REE in addition to Ca and Na, driving the altered betafite compositions towards the A-site cation vacancy apex in Figure 9. Increased hydration is typical of alteration according to Lumpkin and Ewing (1996) and if the lower analytical total for the SK yellow betafite (91.99%) as compared with the SK brown betafite (95.54%) is a reflection of increased hydration, then the Rössing data appears consistent. Certainly, the darker turbid zones in BSE images of 90-24A, which coincide with fluid inclusion trails through the crystal, show increased silica with up to 25 at%. Lumpkin and Ewing (1996) described turbid areas in betafite that show mixtures of anatase, pyrochlore and liandratite (UNb_2O_8), but our analyses do not show this for 90-24A. Only one analysis from within a pyrochlore (90-4.6), suggests that liandratite may occur in some of our samples.

Table 5: REE data obtained by laser ablation ICPMS (analyst Anton le Roux - University of Cape Town)

	A3	A3	A3	A3	A3	A3	B1	B1	B1	B1	B1	A4	A4	A4	A4
	Brn	Brn	Brn	Brn	Brn	Brn	Brn	Brn	Brn	Brn	Brn	Yell	Yell	Yell	Yell
La	319	1984	8635	491	6265	12792	4682	11700	7912	7663	7361	2066	468	1384	2146
Ce	198	1472	33158	4451	28989	46095	26644	41557	31981	30106	29637	10393	3453	6631	10433
Pr	321	2884	4303	1375	4438	6435	4325	5904	4369	4280	3947	1800	698	1201	1551
Nd	131	1366	15683	7665	18859	27183	17877	23273	16887	17611	14704	7962	3424	5470	6343
Sm	305	4369	4685	2430	5240	8355	4717	6317	4209	4967	3456	2141	1031	1466	1734
Eu	150	359	249	291	314	578	249	350	236	279	209	119	66	126	93
Gd	182	3649	3197	1490	4182	7664	3442	4974	3131	4013	2403	1595	776	792	1363
Tb	396	867	1004	322	967	1812	786	1175	713	962	550	361	180	169	320
Dy	253	5981	7559	2031	6652	12595	5302	8070	4836	6638	3710	2470	1225	1026	2204
Ho	518	1250	1638	402	1432	2661	1098	1704	1025	1407	784	526	261	188	467
Er	146	3682	5403	1098	4165	7749	3160	4932	3017	4164	2323	1535	765	502	1362
Tm	241	628	1204	165	710	1324	534	861	505	731	397	252	128	82	235
Yb	173	4655	10258	1115	5089	9450	3869	6342	3725	5433	2955	1799	932	579	1705
Lu	210	557	1209	130	619	1139	455	748	450	646	366	222	115	63	206
tot	515	5925	98183	23446	87922	145834	77141	11790	82997	88902	72801	33242	13523	19678	30163
Wt%	5.1	5.93	9.82	2.34	8.79	14.58	7.71	11.79	8.30	8.89	7.28	3.32	1.35	1.97	3.02

Previous authors (e.g., Chakhmouradian and Mitchell, 1999; Ohnenstetter and Piantone, 1992) have suggested that A-site cation deficiency is related to the U or Th content of pyrochlore group minerals. Our data shows that this is not the case for betafite in terms of U or Th content (cations). Rather, it appears the cation-deficiency in the A-site is related to depletion of Ca and Na from the pyrochlore structure. This has implications for the stability of U within betafite.

The SH area at Rössing is unlikely to be mined for uranium because it is difficult to leach uranium from betafite in the metallurgical processing. Conversely, artificial materials of betafite composition are potential repositories for the containment of radioactive waste. The titanite ceramic designed for disposal of partially reprocessed nuclear fuel elements consists of betafite of near ideal stoichiometry ($CaUTi_2O_7$) as a major phase (Ball *et al.*, 1989). Our studies indicate that the long-term stability of the natural analogue of the ceramic may be partly governed by leaching of Ca. Alteration appears to be linked to A-site cation mobility and loss of Ca and REE, whereas the least mobile A-site cations is U, which is effectively retained in the betafite. Since the Rössing betafites are *c*. 500 million years old our results concur with Lumpkin and Ewing (1996) that a titanite ceramic of betafite composition is an effective repository for actinide waste disposal.

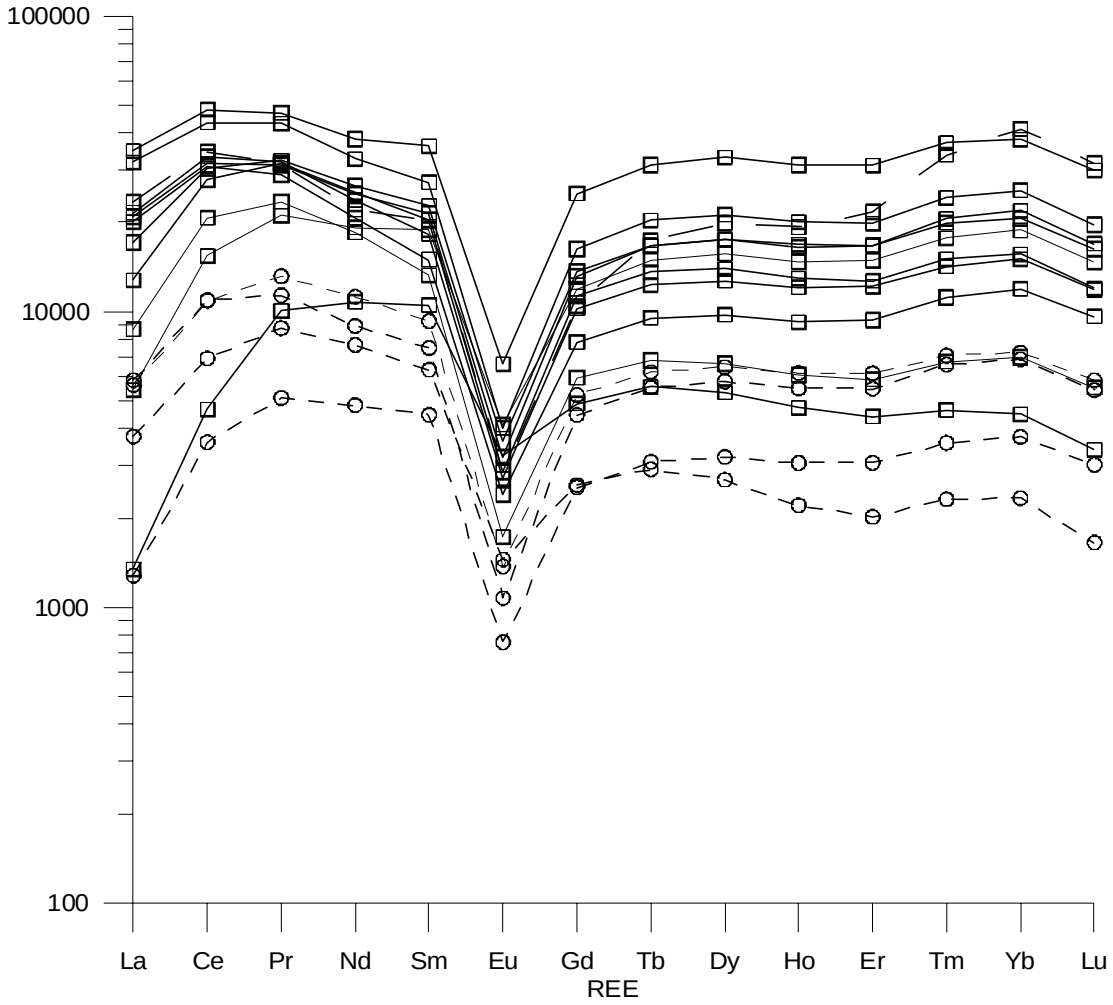

Figure 10. *REE variation diagrams for betafite grains; values in ppm are chrondrite-normalised using the data of Taylor and McLennan (1985). Solid circles represent yellow betafite analyses while crosses are data from brown betafites.*

CONCLUSIONS

In betafite, the principle A-site cations are Ca and U, whereas the A-site occupancy in pyrochlore is dominated by Ca with significant variations in Si, Fe, Y and U content. There may be considerable cation deficiency in the A-site for both betafite and pyrochlore with vacancy varying from 0.1 to 1 atoms pfu. Brown betafite shows the highest A-site occupancy and yellow betafites show the highest A-site vacancies. This vacancy is linked to loss of Ca and Na, whereas the uranium content is more or less constant. Brown betafite has close to full A-site occupancy and <14.5 wt% REE's, whereas altered yellow betafite has > 1 atom pfu vacancy and 1 - 3.5 wt% REE. This A-site vacancy in yellow betafite is linked to loss of Ca, Na and REE, whereas the U has been retained. Artificial ceramics of betafite composition are therefore potential repositories for the containment of radioactive waste.

ACKNOWLEDGEMENTS

This work was conducted mainly as a M. Sc. project by DAH at the University of St. Andrews, funded by GeoMetallica and the University of St. Andrews. The authors would like to thank

Rob Ixer for fieldwork assistance and never-failing good humour and Fred Hubbard for discussion. The Mining Geology Department in Rössing Uranium Limited is acknowledged for their continuing help and support and the Geological Survey of Namibia is thanked for facilitating the research. This paper was completed at the University of the Witwatersrand, and was supported by Grant Cawthorn and by research funds made available from the Amplats, Impala and Lonmin mining companies in South Africa.

REFERENCES

Berning, J. (1986). The Rössing uranium deposit, South West Africa/Namibia. *In*: Anhaeusser, C.R. and Maske, S. (Eds.) *Mineral Deposits of Southern Africa, Vol. II.* Geological Society of South Africa, Johannesburg, pp.1819-1832.

Brandenberger, E. (1931). Die Kristallstruktur von Koppit. *Z. Kristallogr.*, **76**, 322-334.

Chakhmouradian, A.R. and Mitchell, R.H. (1998). Lueshite, pyrochlore and monazite-(Ce) from apatite-dolomite carbonatite, Lesnaya Varaka complex, Kola peninsular, Russia. *Mineralogical Magazine*, **62**, 769-782.

Crowson, P. (2001). *Minerals Handbook 2000-2001*. Mining Journal Books Ltd. Edenbridge UK, 487 pp.

Ewing, R. C. and Ehlmann, A.J. (1975). Annealing study of metamict, orthorhombic, rare earth, AB_2O_6-type, Nb-Ta-Ti oxides. *Canadian Mineralogist,* **13**, 1-7.

Gasperin, M. (1960). Contribution à l' etude de quelques oxides doubles que forme le tantale avec l'étain, l'uranium et le calcium. *Bulletin Societé francais Minéral. Cristallogr.,* **83**, 1-21.

Gaertner, H.R. (1930). Die Kristallstrukturen von Loaprit und Pyrochlor. *Neues. Jahr. Mineral., Beil-Band,* **61**, Abt. A, 1-30

Ball, C.J., Buykx, W.J., Dickson, F.J., Hawkins, K., Levins, D.M., Smart, R.St.C., Smith, K.L., Stevens, G.T., Watson, K.G., Weedon, D. and White, T.J. (1989). Titanite ceramics for the stabilisation of partially reprocessed nuclear fuel elements. *Journal of the American Ceramic Society*, **72**, 404-414.

Herd, D. A. (1996). *Geochemistry and mineralisation of alaskite in selected areas of the Rössing Uranium Mine, Namibia.* M. Sc. dissertation (unpubl.), University of St. Andrews, Scotland, 144 pp.

Hogarth, D.D. (1961). A study of pyrochlore and betafite. *Canadian Mineralogist,* **6**, 610-633.

Hogarth , D. (1977). The Pyrochlore Group. *American Mineralogist,* **62**, 430-410.

Hogarth, D.D. (1989). Pyrochlore, apatite and amphibole: distinctive minerals in carbonatite. *In:* Bell, K. (Ed.), *Carbonatites, Genesis and Evolution.* Unwin Hyman, London, 105-148.

Hogarth, D.D., Williams, C.T. and Jones, P. (2000). Primary zoning in pyrochlore group minerals from carbonatites. *Mineralogical Magazine,* **64**, 683-697.

Lacroix, A. (1912). Sur un groupe de niobo-tantalites cubiques (radioactifs) des pegmatites de Vakinankaratra. *Bulletin Societé francais Minéralogie*, **35**, 84-92.

Le Bas, M.J. and Streckeisen, A.L. (1991). The IUGS systematics of igneous rocks. *Journal of the Geological Society, London*, **148**, 825-833.

Lumpkin, G.R., Chakoumakos, B.C. and Ewing, R.C. (1986). Mineralogy and radiation effects of microlite from the Harding pegmatite, Taos County, New Mexico. *American Mineralogist,* **71**, 569-588.

Lumpkin, G.R., Ewing, R.C. and Eyal, Y. (1988). Preferential leaching and natural annealing of alpha-recoil tracks in metamict betafite and samarskite. *Journal of Materials Research,* **3**, 357-368.

Lumpkin, G.R. and Ewing, R.C. (1996). Geochemical alteration of pyrochlore group minerals: betafite subgroup. *American Mineralogist,* **81**, 1237-1248.

Mazzi, F. and Munno, R. (1983). Calciobetafite (new mineral of the pyrochlore group) and related minerals from Campi Flegrei, Italy; crystal structures of polymignyte and zirkelite: comparison with pyrochlore and zirconolite. *American Mineralogist,* **68**, 262-276.

Mitchell, R.H. and Kjarsgaard, B.A. (2003). Solubility of niobium in the system $CaCO_3$-$Ca(OH)_2$-$NaNbO_3$ at 0.1 GPa pressure. *Contributions to Mineralogy and Petrology,* **144**, 93-97.

Nex, P.A.M. (1997). *Tectono-metamorphic setting and evolution of granitic sheets in the Goanikontes area, Namibia.* Ph.D. thesis (unpubl.), National University of Ireland, University College, Cork, 322 pp.

Nex, P.A.M., Kinnaird, J.A. and Oliver, G.J.H. (2001). Petrology, geochemistry and uranium mineralisation of post-collisional magmatism around Goanikontes, southern Central Zone, Damara Orogen, Namibia. *Journal of African Earth Sciences,* **33**, 481-502.

Nex, P., Herd, D. and Kinnaird, J. (2002). Fluid extraction from quartz in sheeted leucogranites as a monitor to styles of uranium mineralisation: an example from the Rössing area, Namibia. *Geochemistry: Exploration, Environment, Analysis,* **2**, 83-96.

Ohnenstetter, D. and Piantone, P. (1992). Pyrochlore-group minerals in the Beauvoir peraluminous leucogranite, Massif Central, France. *Canadian Mineralogist,* **30**, 771-784.

Smith, D.A.M. (1965). The geology of the area around the Khan and Swakop rivers in South West Africa. *Memoir, Geological Survey and Department of Mines, South West Africa, Series* **3**, 113 pp.

Taylor, S.R. and McLennan, S.M. (1985). *The Continental Crust: its Composition and Evolution*. Blackwell, Oxford.

Tindle, A.G. and Breaks, F.W. (1998). Oxide minerals of the Separation Rapids rare-element granitic pegmatite group, Northwestern Ontario. *Canadian Mineralogist,* **36**, 609-635

Von Backström , J.W. (1970). The Rössing uranium deposit near Swakopmund, South West Africa: a preliminary report. *Uranium Exploration Geology, IAEA Report* **IAEA -PL-391/12** Vienna, 143-150.

Wall, F., Williams, C.T., Wolley, A.R. and Nasraoui, M. (1996). Pyrochlore from weathered carbonatite at Lueshe, Zaire. *Mineralogical Magazine,* **60**, 731-750.

Williams, C.T., Wall, F., Woolley, A.R. and Phillipo, S. (1997). Compositional variation in pyrochlore from the Bingo carbonatite, Zaire. *Journal of African Earth Sciences,* **25**, 137-145.

_____oOo_____